Invited Overview

Terahertz Functional Devices Based on Photonic Crystal and Surface Plasmon Polaritons

Dongxiao Yang [1, 2*], Tao Li [1], Lei Rao [1], Song Xia [1], Le Zhang [1]

[1] Zhejiang University, Department of Information Science and Electronic Engineering, 310027 Hangzhou, PR China
[2] Zhejiang University, Research Center for Terahertz Technology, Hangzhou 310027, PR China
*Email: yangdx@zju.edu.cn

Abstract: Terahertz functional devices are as important as sources and detectors in many terahertz systems. Photonic crystal structures designed with band gaps and surface plasmon polaritons on corrugated metallic surfaces are two excellent ways to control the propagation of terahertz wave, which is suitable for designing and fabricating various kinds of functional devices in terahertz region. Some typical terahertz devices based on photonic crystals and surface plasmon polaritons are investigated in this paper, such as terahertz wideband filter, terahertz band-stop filter, terahertz waveguide, terahertz resonant cavity.

1. Introduction

Nowadays, the terahertz (THz) frequency region, generally referring to the electromagnetic spectrum from 100 *GHz* to 10 *THz*, has drawn much attention because of its unique properties and many demonstrated applications [1]. However, technical challenges still exist and some typical functional devices such as filters, waveguides, polarizers, and modulators are still required for further research.

Photonic crystal (PC) firstly presented in 1987 by Yablonovitch is a sort of periodic structure which can afford to completely control the propagation of light [2]. PCs with photonic band gaps can be designed and constructed, in order to prevent light from propagating in certain directions at given frequencies. Band gaps and defects in PCs can be combined to form filters [3], waveguides [4] and other devices [5]. Particularly, PCs allow the useful properties of filters and waveguides to be generalized and scaled to encompass a wider range of frequencies. Therefore,in THz frequency region, PCs have become the essential structures when designing and fabricating different kinds of functional devices.

Since Ebbesen *et al*. found extraordinary optical transmission through sub-wavelength holes array [6], worldwide researches have been done and several reviews have been given to demonstrate its physical mechanism and possible applications [7-8]. It is generally believed that

the surface plasmon polaritons (SPPs), excited by the incident light and transmitted on the metal surface, can enhance the transmissions through holes array [9-10]. At lower frequencies like terahertz and microwave regimes where metal is assumed to be a perfect electric conductor and SPPs cannot be supported, enhanced transmissions were observed [11-12]. It has been theoretically [13] and experimentally [14] proved that spoof SPPs can be excited on the corrugated perfect electric conductor surfaces. Based on spoof SPPs, band-pass filters and waveguides can be easily designed in THz region.

2. Terahertz filters

2.1 Band-pass filter based on surface plasmon polaritons

By utilizing the characteristics of spoof SPPs, THz transmission filters can be designed and manufactured by perforating metal films with various geometric shapes. J. W. Lee *et al*. have found that plasmonic structures with different geometric shaped holes are extremely versatile, dependable, easy to control and easy to make THz filters, supporting over 99% transmission at specific frequencies determined by geometric shapes [15]. By puncturing a series of nanoresonator arrays in a thin metallic film, H. R. Park *et al*. have designed an ultrabroadband THz filter with one decade width between 0.2 and 2.0 *THz* [16]. A passband filter based on metal-dielectric-metal sandwich plasmonic structure with bandwidth of 500 *GHz* centered at 1.25 *THz* has been realized by J. G. Han *et al*. [17]. However, the structures of these two broadband THz filters are relatively complicated.

Terahertz wideband filters have been designed and experimentally verified based on double-layered metal hole arrays [18-19]. The schematic of the considered double-layered metal air hole array is shown in Fig. 1. The parameters of the double-layered metal hole array are $d = 300 \ \mu m$, $h_m = 30 \ \mu m$, $a = 180 \ \mu m$, $h_s = 120 \ \mu m$, $\varepsilon = 1$, and for the single-layered metal hole array the parameters of d, h_m, a and ε are the same.. Figure 2 shows the zero-order transmission spectra of the single-layered and double-layered metal hole arrays, which were calculated using rigorous mode-matching method. It can be found that there is a deep minimum locating at 1.0 *THz* in both transmission spectra. This minimum should be caused by Wood anomaly [20]. There are three anomalous peaks at 0.788 *THz*, 0.863 *THz* and 0.993 *THz* in the spectrum of the double-layered metal hole array and two anomalous peaks at 0.877 *THz* and 0.997 *THz* in the spectrum of the single-layered metal hole array. These peaks are associated with the coupling of leaky surface electromagnetic modes via the holes between interfaces of the holey metal films. Double-layered metal hole array is a good option for wideband filters.
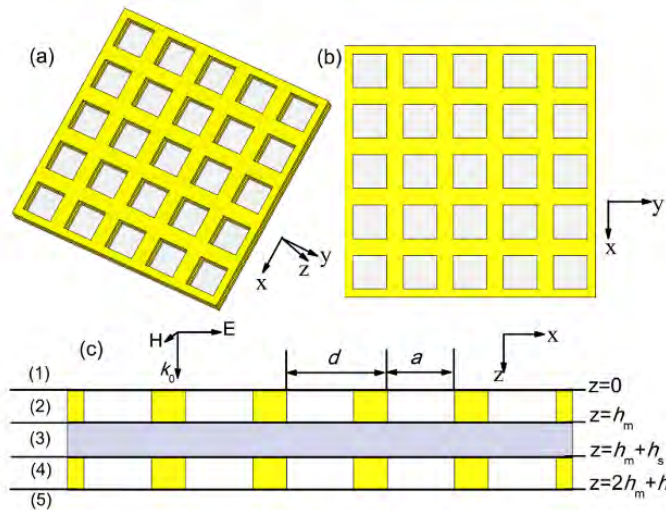
Fig. 1 Schematic of the considered double-layered metal air hole array. (a) Three dimensional view, (b) and (c) cross-sectional views.
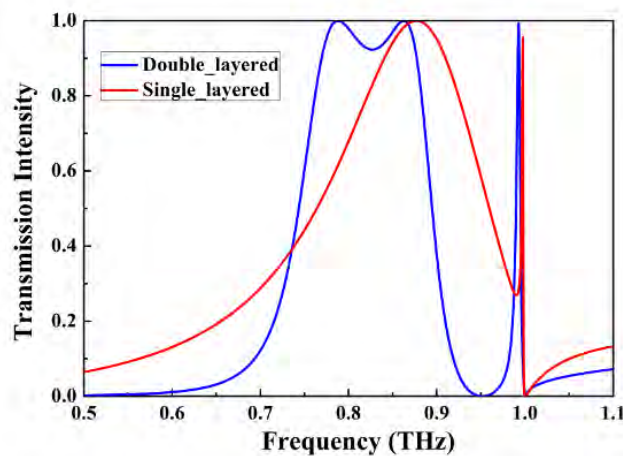

Fig. 2 Zero-order transmission spectra of the single-layered and double-layered metal hole arrays.

Based on the simulation results, wide pass band filters have been designed and fabricated at THz frequency region. Two samples made of double brass layers with square lattices of air circular holes were fabricated with the same parameters: $d = 300 \ \mu m$, $h_m = 30 \ \mu m$, $r = 90 \ \mu m$, where r is the radius of the air hole, as shown in Fig. 3. The sample area ratio of air hole to metal is 28%. The distance h_s in Sample_A is 130 μm and in Sample_B is 120 μm. The substrate between the two brass layers is the air with the relative permittivity ε of 1.
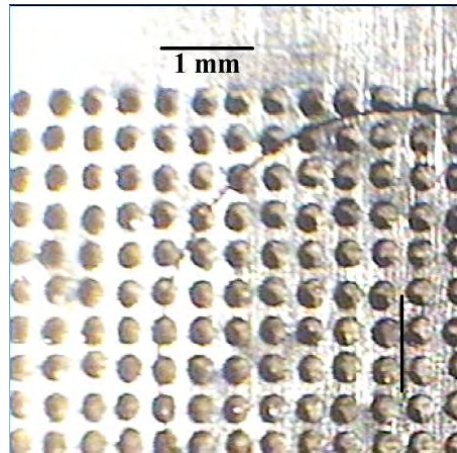
Fig. 3 Sample picture of band-pass filter based on SPPs.

THz waves through these two samples and reference with the same aperture were measured by broadband THz-TDS, respectively. The transmission spectra of the reference and the samples shown in Fig. 4(a) are derived by FFT of the waveforms, which is also measured in the experiments. The inset shows the schematic of Sample A. Figure 4(b) shows the transmittances of Sample A and Sample B where the transmittance is defined as the transmission spectrum of the sample, dividing the transmission spectrum of the reference. Passbands with the center frequency located at 0.8 *THz* and FWHM around 400 *GHz* are both realized in the two samples. Two times transmission enhancement has obtained for the samples at the frequency near 0.8 *THz* according to Fig. 4(b).
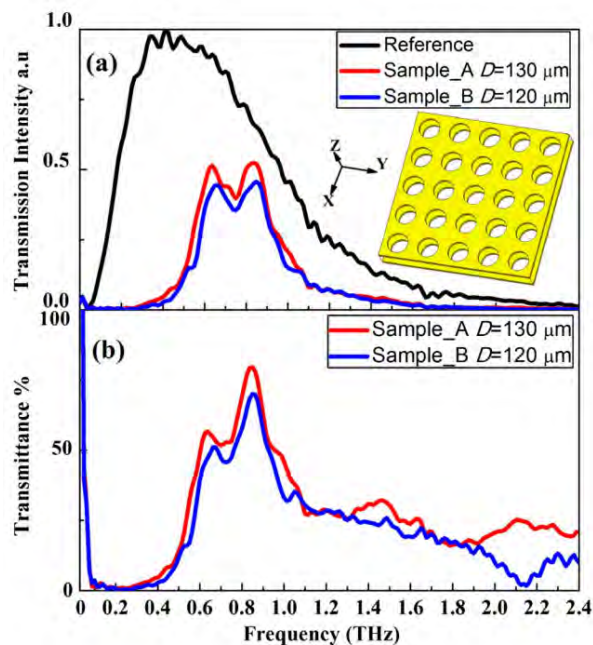

Fig. 4 (a) Frequency spectra of the reference and the samples derived by FFT of the waveforms measured in the experiments. The inset shows the schematic of Sample. (b) Transmittances of Sample A and Sample B.

2.2 Band-stop filter based on surface plasmon polaritons

A stop band filter [21] is composed of two identical parallel metallic plates textured with rectangular groove arrays of period *a*, as shown in Fig. 5. The length of the grooves is infinite in x direction. The width and depth of the rectangular grooves are *l* and *d*, respectively. The gap width of the two surfaces is *w*. THz waves propagate between the two identical groove arrays.
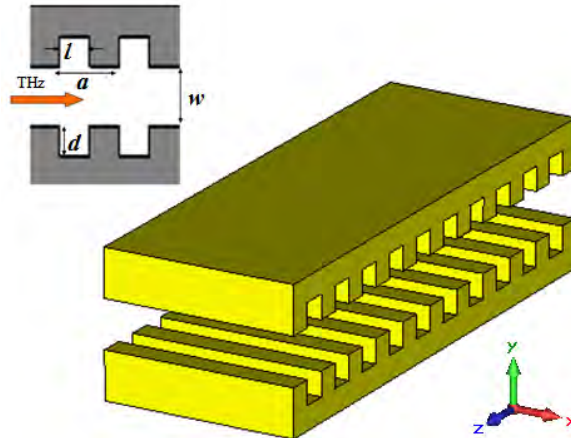

Fig. 5 Layout of the stop band filter based on SPPs.

Simulation results shown in Fig. 6 render the dispersion relation of the gap modes, propagating between two identical groove arrays. The frequency and wave vector are plotted in the dimensionless units $\omega a/2\pi c$ and $ka/2\pi$. The dimensionless unit frequency is equivalent to a/λ, where λ is the vacuum wavelength (given by $\lambda = 2\pi c/\omega$). In this case, the geometric parameters of the grooves are $l = d = 0.5a$. The gap width of the two metallic plates is $w = 2a$. There is a band gap ranging from $0.315c/a$ to $0.350c/a$ in the dispersion relation (the yellow strip in Fig. 6), which means that a stop band filter with bandwidth of $0.035c/a$ is achieved. By changing the gap width *w* and groove depth *d*, different filtering bandwidths with different center frequencies can be achieved.
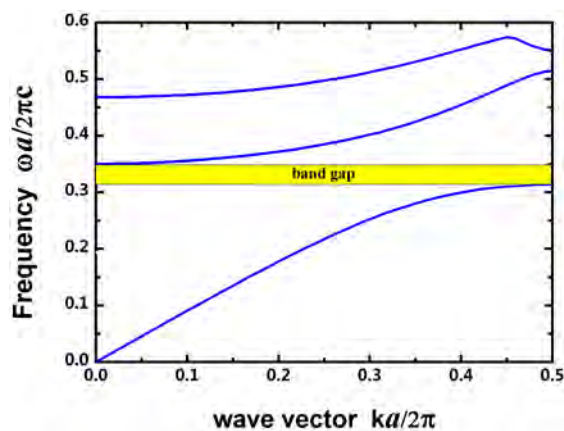

Fig. 6 Dispersion relation of the guided electromagnetic modes of the filter. The yellow zone represents a band gap ranging from $0.315c/a$ to $0.350c/a$.

2.3 Band-stop filter based on photonic crystal

Photonic crystals have band gaps where light can not propagate. Based on photonic band gaps, another stop band filter can be easily designed. N. Jukama and M. Sherwin fabricated a two-dimensional THz PC stop band filter from Si using deep reactive ion etching. Stop bands with transmittance <1% and widths >200 *GHz* were observed near 1 *THz* [22]. Using electrochemical etching, S. Z. Lo and T. Murphy fabricated a structure composed of alternating high- and low-index layers that achieves 93% power reflectivity at the target wavelength of 1.17 *THz*, with a stop band of 0.26 *THz* [23].

A band-stop filter sample is fabricated on high-resistivity silicon slab with triangular lattice constant $a = 0.29$ *mm*, air holes' radius $r = 0.283a$ and thickness $t = a$, as shown in Fig. 7. The sample is experimented with a THz backward wave oscillator whose effective frequency range is from 0.235 to 0.375 *THz*. The radiated THz waves go through an attenuator and two polyethylene lenses first, and then focus on the PC sample. To reduce the measurement noise, a metal sheet is added at the middle position of the sample preventing those waves propagating out of the sample from reaching the detector. Also through two polyethylene lenses, the THz waves emitted from the end of the PC sample at last focus on the pyroelectric detector.
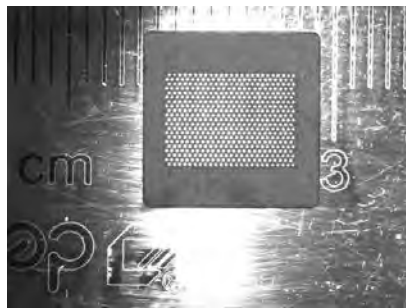

Fig. 7 Sample picture of the band-stop filter based on PC.

The measured transmission spectrum in the frequency range of 0.25～0.35 *THz* is shown in Fig. 8. It can be seen that the transmission spectrum is low from 0.25 to 0.34 *THz*, forming a THz band gap. The illustration shows a wider frequency range of the transmission spectrum. The blue shaded part is the theoretically calculated PC band gap, which is in good agreement with the experimental results. Using this band gap, the band-stop function is realized.
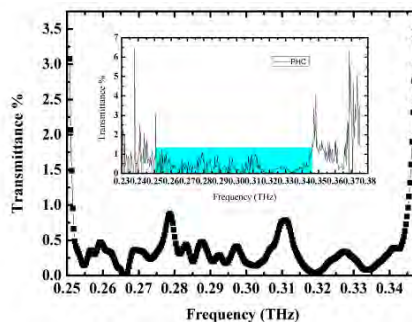

Fig. 8 Measured transmission spectrum of the band-stop filter based on PC.

3. Terahertz waveguides

3.1 Photonic crystal slab waveguide

Defects in PC slabs can be used to form waveguides and cavities. Z. Jian *et al.* studied the broadband coherent transmission of two-dimensional PCs consisting of a hexagonal array of air holes in a dielectric slab in a planar waveguide [24]. B. Chen calculated the results which indicate that for arbitrary-angle bends of this waveguide with very small curved radii no more than two wavelengths, a very high transmission (>98.5%) is observed for a broad enough bandwidth [25].

A waveguide sample on high-resistivity silicon slab has been fabricated with triangular lattice constant $a = 0.29$ *mm*, air holes' radius $r = 0.283a$ and thickness $t = a$. This PC slab waveguide [26] is formed by removing a single row of air holes along the Γ- K direction in the center of PC slab, as shown in Fig. 9.
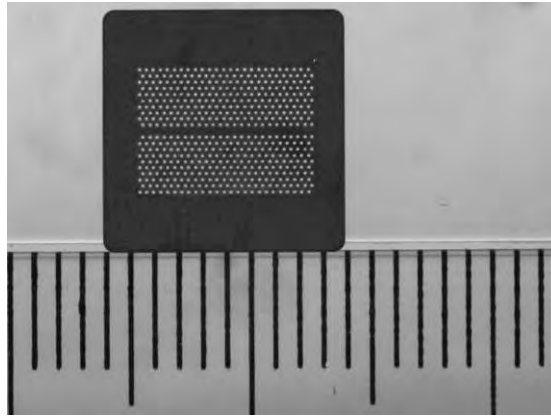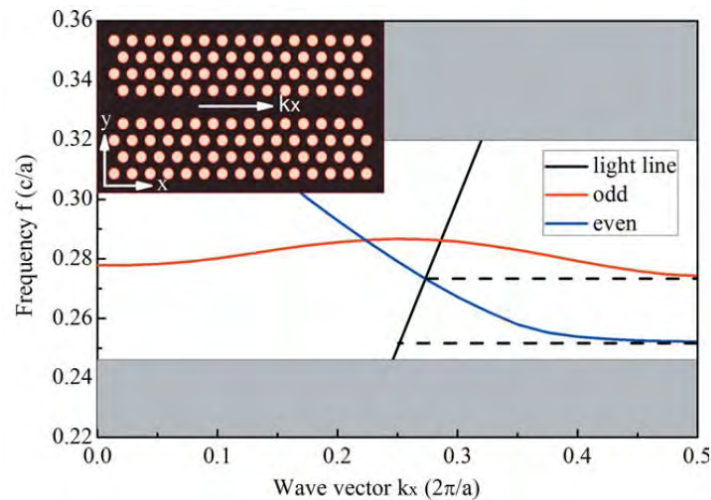

Fig. 9 Sample picture of PC slab waveguide.

Fig. 10 Band diagram of TE-like modes for the PC waveguide along Γ-K direction. The inset shows the schematic diagram of the PC waveguide.

The band diagram calculated by the three-dimensional finite difference time domain method of TE-like (electric field is parallel with the slab plane) modes for the PC waveguide

along Γ-K direction with normalized frequency (c/*a*) is shown in Fig. 10. The black line is the light line and the gray shadows are the leaky regions. It can be found that there are two waveguide modes with even and odd symmetries appearing within the band gap. Below the light line, both two waveguide modes are confined horizontally by the band gap and vertically by the index guiding. Therefore, the electromagnetic waves of these two waveguide modes are restricted to propagate within the line-defect and should be lossless in an ideal PC waveguide without imperfections [27]. As indicated by the dash lines, a single mode with even symmetry exists below the light line and its frequency range is from 0.252 (c/*a*) to 0.273 (c/*a*). Parts of the waveguide modes existing above the light line can be extended into the air, which will bring large out-of-plane radiation loss.

The transmission spectra of the PC waveguide were measured by a submillimeter spectrum system which includes THz backward wave oscillator and pyroelectric detector. Figure 11(a) shows the transmittance spectrum of the PC waveguide sample. The calculated band diagram of the PC waveguide with the lattice constant of 290 *μm* in Fig. 10 is redrawn in Fig. 11(b) to give a comparison with the experimental results. From 0.25 to 0.26 *THz*, the transmittance is low because no waveguide modes are supported. From 0.26 to 0.268 *THz,* the transmittance increases significantly due to the appearance of the even waveguide mode. As frequency increases further, the transmittance decreases because the waveguide mode approaches to the light line. The fabrication errors can lead the electromagnetic waves of the waveguide mode near the light line coupled into the air and increase the radiation loss. In addition, the large impedance mismatch between the small group velocity of the waveguide mode in the PC waveguide and the electromagnetic wave velocity in the free space will also bring coupling loss. The experimental results show the reasonable agreement with the circulated results.
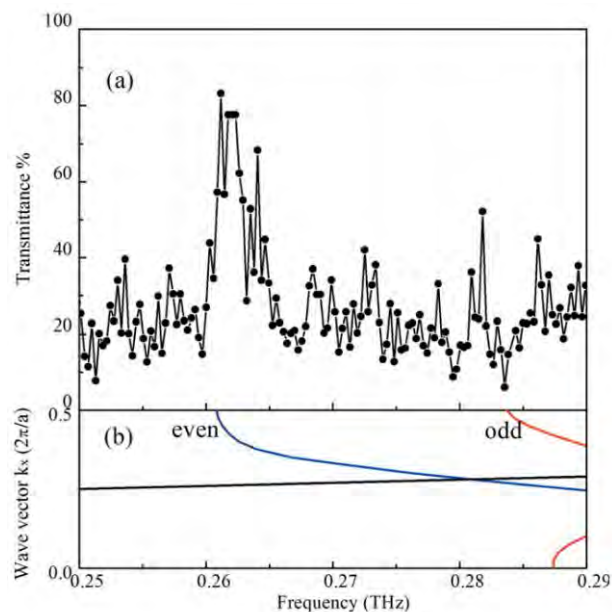

Fig. 11 (a) Transmittance spectrum of the PC waveguide sample measured by submillimeter spectrum system. (b) Redraw of Fig. 10 with the lattice constant of 290 *μm*.

3.2 Waveguide based on surface plasmon polaritons

SPPs can propagate on periodically corrugated metal surfaces. S. A. Maier *et al.* showed how the dispersion relation of SPPs propagating along a perfectly conducting wire could be tailored by corrugating its surface with a periodic array of radial grooves [28]. C. R. Williams *et al.* reported direct measurements of the propagation and confinement of THz electromagnetic surface modes tightly bound to flat plasmonic metamaterials that consist of metal surfaces decorated with two-dimensional arrays of subwavelength-periodicity pits [29]. L. F. Shen *et al.* investigated numerically the characteristics of SPPs sustained by two-dimensional arrays of metallic pillars protruding out of planar metal surfaces at THz frequencies [30].

Utilizing the prosperity that the SPPs can propagate on the surface of metal fabricated periodic subwavelength arrays, a waveguide based on spoof SPPs is designed in the THz range. Figure 12 shows the schematic diagram of metal waveguide patterned with subwavelength square periodic lattice arrays and its simulation results. The corresponding parameters are: $d = 0.3$ *mm*, $a = 0.8d = 0.24$ *mm*, $t = 1.2d = 0.36$ *mm*, where d is the periodicity, a is the side length of square hole and t is the depth of the holes. Figures 12(a) and 12(b) illustrate the planform of x-y plane and side elevation of x-z plane, in which the metal slabs are used to excite and couple the SPPs existing on the metal surface.

The electric field distribution E_z is displayed in Fig. 12(c) and Fig. 12(d), where the former represents E_z on a smooth metal while the latter represents E_z on a metal with periodic arrays. From Fig. 12(c), it is obvious that no SPPs are excited on the metal surface and merely ordinary electromagnetic wave propagates in air. However, Fig. 12(d) indicates that there are SPPs propagating along the interface of metal and air. Further, the SPPs dispersion along x direction at the metal/air interface is presented in Fig. 12(e), showing a working frequency range of $0 \sim 0.44$ *THz*. By means of 3D simulation technology, the THz transmission curve of the waveguide is obtained in Fig. 12(f), indicating that SPPs can propagate at the surface of the metal structure in $0.35 \sim 0.45$ *THz*. Clearly, the lower transmittance part of the transmission curve is adjacent to the light cone and corresponding energy can be easily coupled into the air, leading to no SPPs generated on the metal/air interface. Nevertheless, the higher transmittance part of the transmission curve is far from the light cone, illustrating that SPPs are excited and can stably propagate along the surface of metal with little energy leaking into the air.

As it is analyzed above that the SPPs play an important role in the THz transmission for a subwavelength periodic arrays, it is possible to design waveguide with different frequency selection in THz range by adjusting the parameters of the structure.
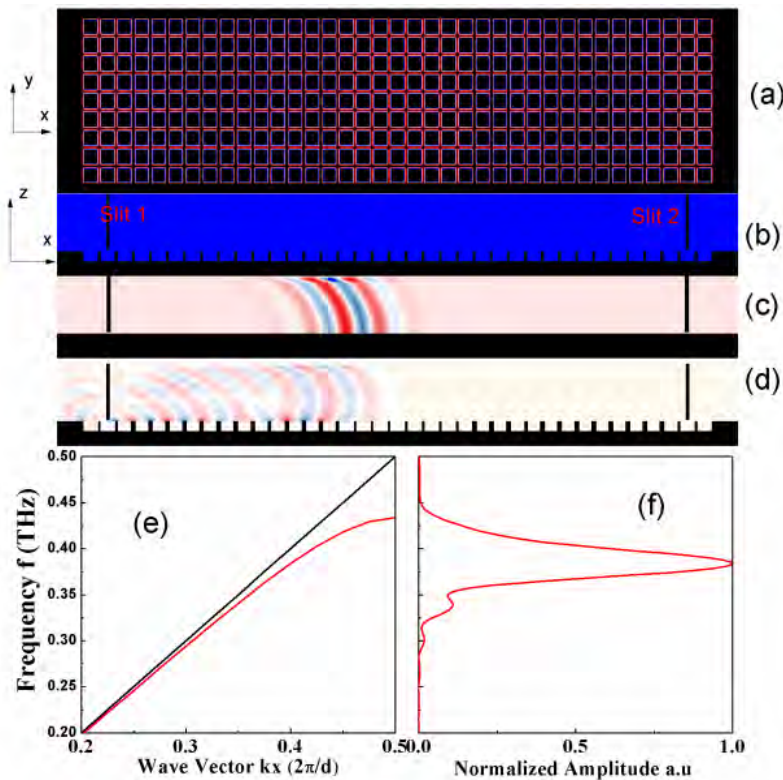
Fig. 12 Diagram of structure with square periodic hole arrays on the metal and its simulation graph.

4. THz resonant cavity

A two-dimensional PC cavity is fabricated starting from high-resistivity silicon slab with thickness of 0.29 *mm*. After cutting it into 10 x 10 *mm* square blocks, laser micromachining technology is utilized to drill air holes on the slab according to the PC design pattern. A cavity with three missing air holes in the center of the slab and two line defect (bus line and drop line) waveguides fabricated by missing a row of air holes on each side of the cavity is done. The triangular periodicity and air holes radius are chosen as $a = 0.29$ *mm* and $r = 0.283a$, respectively, which is shown in Fig. 13.

Originally, this structure can be used as a cavity if the electromagnetic wave is inputted at the waveguide entrances and emitted from the top of the cavity. Also, it can be used as a drop filter if the electromagnetic wave is inputted at one entrance of the waveguides and emitted from the other's exit as shown in Fig. 13 in red arrowheads. The FDTD method is used to calculate the transmission spectrum of the structure which predicts $Q = 962$ with center frequency at $0.269(c/a)$ in Fig. 14. The spectrum has been normalized by setting the peak equal to one.
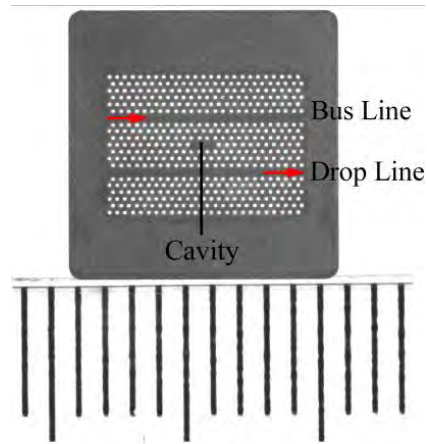
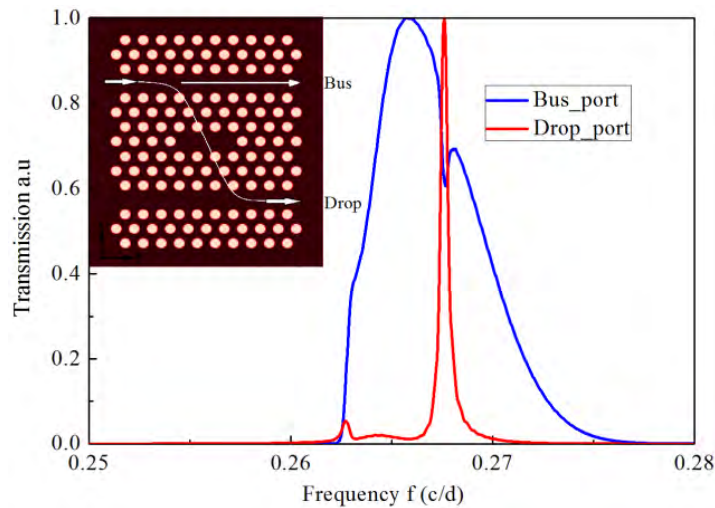Fig. 13 Sample picture of the two-dimensional PC cavity.

Fig. 14 Transmission spectrum of the PC cavity from the bus line to the drop line.

5. Conclusion

The study on some typical terahertz functional devices based on photonic crystals and surface plasmon polaritons have been presented in this paper. THz filters, THz waveguides and THz resonant cavity are analyzed by simulations and experiments. Based on these results, more terahertz devices and their applications can be forecasted.

Acknowledgements

References

[1] I. Hosako, N. Sekine, M. Patrashin, S. Saito, K. Fukunaga, Y. Kasai, P. Baron, T. Seta, J. Mendrok, S. Ochiai and H. Yasuda, At the dawn of a new era in terahertz technology, *Proceedings of the IEEE*, 95, 1611-1623, (2007).

[2] Eli Yablonovitch, Inhibited Spontaneous Emission in Solid-State Physics and Electronics, Phys. Rev. Lett. 58, 2059-2062, (1987)

[3] R. Mendis, A. Nag, F. Chen and D. M. Mittleman, A tunable universal terahertz filter using artificial dielectrics based on parallel-plate waveguides, *Applied physics letters*, 97, 131106, (2010).

[4] A. H. B. Ghasemi and H. Latifi, Localized modes in a defectless photonic crystal waveguide at terahertz frequencies, *Optics Letters*, 37, 2727-2729, (2012).

[5] T. Okada and K. Tanaka, Photo-designed terahertz devices, *Scientific Reports,* 1, 121, (2011).

[6] T. W. Ebbesen, H. J. Lezec, H. F. Ghaemi, T. Thio and P. A. Wolff, Extraordinary optical transmission through sub-wavelength holearrays, *Nature*, 391, 667-668, (1998).

[7] C. Genet and T. W. Ebbesen, Light in tiny holes, *Nature*, 445, 39-46, (2007).

[8] F. J. Abajo, Colloquium: Light scattering by particle and hole arrays, *Reviews of Modern Physics*, 79, 1267-1290, (2007).

[9] E. Ozbay, Plasmonics: Merging photonics and electronics at nanoscale dimensions, *Science*, 311, 189-192, (2006).

[10] S. A. Maier and H. A. Atwater, Plasmonics: Localization and guiding of electromagnetic energy in metal/dielectric structures, *Journal of Applied Physics*, 98, 011101, (2005).

[11] X. Xiao, J. B. Wu, Y. Sasagawa, F. Miyamaru, M. Y. Zhang, M. W. Takeda, C. Y. Qiu, W. J. Wen and P. Sheng, Resonant terahertz transmissions through metal hole array on silicon substrate, *Optics Express*, 18, 18558-18564, (2010).

[12] J. W. Lee, T. H. Park, P. Nordlander and D. M. Mittleman, Optimum areal coverage for perfect transmission in a periodic metal hole array, *Applied physics letters*, 97,261112, (2010).

[13] J. B. Pendry, L. M. Moreno and F. J. Vidal, Mimicking surface plasmons with structured surfaces, *Science*, 305, 847-848, (2004).

[14] A. P. Hibbins, B. R. Evans and J. R. Sambles, Experimental verification of designer surface plasmons, *Science*, 308, 670-671, (2004).

[15] J. W. Lee, M. A. Seo, D. J. Park, D. S. Kim, S. C. Jeoung, C. Lienau, Q.H. Park and P. C. M. Planken, Shape resonance omni-directional terahertz filters with near-unity transmittance, *Optics Express*, 14, 1253-1259, (2006).

[16] H. R. Park, Y. M. Park, H. S. Kim, J. S. Kyoung, M. A. Seo, D. J. Park, Y. H. Ahn, K. J. Ahn and D. S. Kim, Terahertz nanoresonators: Giant field enhancement and ultrabroadband performance, *Applied Physics Letters,* 96, 121106, (2010).

[17] J. G. Han, J. Q. Gu, X. C. Lu, M. X. He, Q. R. Xing and W. L. Zhang, Broadband resonant terahertz transmission in a composite metal-dielectric structure, *Optics Express,* 17, 16527-16534, (2009).

[18] L. Rao and D. X. Yang, Surface electromagnetic modes contribution to the anomalous terahertz transmission through double-layered metal hole array, *SCIENCE CHINA Information Sciences*, 55, 90-97, (2012).

[19] L. Rao, D. X. Yang, L. Zhang, T. Li and S. Xia, Design and experimental verification of terahertz wideband filter based on double-layered metal hole arrays, *Applied Optics*, 51, 912-916, (2012).

[20] M. Dragoman and D. Dragoman, Plasmonics: Applications to nanoscale terahertz and optical devices, *Progress in Quantum Electronics*, 32, 1-41, (2008)

[21] T. Li, D. X. Yang, L. Rao and S. Xia, A terahertz stop band filter based on two parallel metallic surfaces textured with groove arrays, *Proc. SPIE*, 8195, 81951Q1-6, (2011).

[22] N. Jukama and M. Sherwin, Two-dimensional terahertz photonic crystals fabricated by deep reactive ion etching in Si, *Applied physics letters*, 83, (2003).

[23] S. Z. Lo and T. Murphy, Nanoporous silicon multilayers for terahertz filtering, *Optics Letters*, 34, 2921-2923, (2009).

[24] Z. Jian, J. Pearce and D. M. Mittleman, Defect modes in photonic crystal slabs studied using terahertz time-domain spectroscopy,*Optics Letters*. 29, 2067-2069, (2004).

[25] B. Chen, T. T. Tang and H. Chen, Study on a compact flexible photonic crystal waveguide and its bends, *Optics* Express 17, 5033-5038, (2009).

[26] L. Rao, D. X. Yang and Z. Hong, Guiding terahertz wave within a line defect of photonic crystal slab, *Microwave and Optical Technology Letters*, 54, 2856-2858, (2012).

[27] A. Baron, S. Mazoyer, W. Smigaj and P. Lalanne, Attenuation coefficient of single-mode periodic waveguides, *Physical Review Letters,* 107, 153901, (2011).

[28] S. A. Maier, S. R. Andrews and L. Martı´n-Moreno, Terahertz Surface Plasmon-Polariton Propagation and focusing on Periodically Corrugated Metal Wires. *Physical Review Letters.* 97, 176805, (2006).

[29] C. R. Williams, S. R. Andrews, S. A. Maier, A. I. Fernandez-Dominguez, L. Martin-Moreno and F. J. Garcia-Vidal, Highly confined guiding of terahertz surface plasmon polaritons on structured metal surfaces, *Nature Photonics*, 2, 175-179, (2008).

[30] Z. Gao, L. F. Shen, J. J. Wu, T. J. Yang and X. D. Zheng, Terahertz surface plasmon polaritons in textured metal surfaces formed by square arrays of metallic pillars. *Optics Communications,* 285, 2076–2080, (2012).